Convection in a Fluid Loop

Eleanor Frajka Williams

Abstract

Sandström's conjecture states that a closed steady circulation can only be maintained in a fluid body if the heating is applied at a lower level than the cooling. In the ocean this has been taken to mean that there can not be a purely buoyancy-driven circulation since the primary sources of heat and salt are applied at the surface. Using the one-dimensional fluid loop of Welander with boundary condition of temperature relaxing to warm and cold at the same geopotential, we find that Sandström's conjecture holds; circulation and horizontal heat transport all vanish as the Rayleigh number $R \longrightarrow \infty$ (the limit relevant for the ocean). However, if we specify fixed temperature flux boundary conditions, then contrary to Sandström's conjecture, circulation does not vanish as $R \longrightarrow \infty$. Thus Sandström's conjecture is sensitive to the particular choice of boundary conditions specified. In the case of the ocean, where salinity and sensible heat also play a role in forcing the system, it is not clear that fixed temperature rather than fixed flux boundary conditions at the surface are appropriate.

This system of horizontal convection in a loop is stable, but becomes chaotic as the heat sources are rotated from horizontal to vertical positions (heating at the bottom and cooling at the top). We determine the orientation of the heating and cooling at which this transition to chaos occurs. We also show how the strength of the circulation responds to different positioning of heating and cooling.

1 Introduction

Oceanographers have long debated whether or not there can exist a purely buoyancy-driven circulation in the ocean. Roots of the discussion trace back at least as far as J.W. Sandström in 1908 who, assuming the ocean circulation worked like a heat engine, concluded that there cannot exist a circulation unless the heating occurs below the cooling, a result sometimes known as Sandström's Theorem. We will call it Sandström's conjecture. The statement has since been formalized to include effects of friction and viscosity, which Sandström did not consider, and can be stated as

> *Sandström's Conjecture:* "If a viscous and diffusive fluid is nonuniformly heated from the same level then in the limit $\kappa \longrightarrow 0$ with ν/κ fixed, the motion in the fluid also disappears," (1).

Oceanographers have inferred from Sandström's conjecture that turbulent mixing rather than buoyancy drives the global conveyor belt (meridional overturning circulation) and that there must be a mechanical energy source to drive the raising of cold water such as wind or tides (2). Then the meridional overturning circulation is just a salt and heat conveyor belt riding on the wind- and

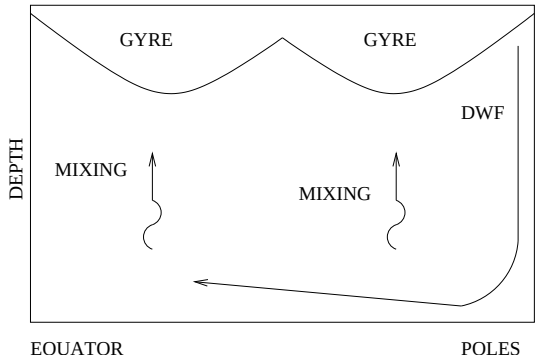

Figure 1: The story: A picture of the global ocean circulation. The wind-driven gyres are near the surface, deep water formation (DWF) at the poles. Mixing due to wind stress and tidal dissipation is required to bring heat down to the abyss to stratify the abyssal ocean. If you remove the mixing, the abyss will fill up with cold water and there will be no circulation.

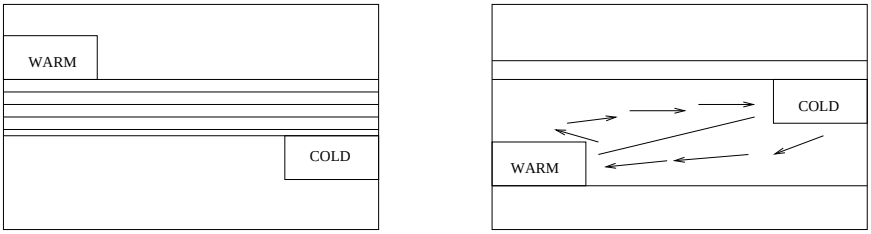

(a) Type I (b) Type III

Figure 2: Convection in a box with heating and cooling sources placed at different levels. Adapted from Defant (4).

tidally-driven circulation (3). Figure 1 shows the ocean circulation with the wind-driven gyres at the top, with deep convection at the poles closed by interior mixing. In the absence of this mixing, Munk and Wunsch say the ocean would just fill up with cold water and have a very shallow, warm circulation near the surface (2).

Paparella and Young (2002) examined horizontal convection in a 3-D ocean with fixed temperature boundary conditions (5). They showed that dissipation vanishes as diffusivity vanishes using the maximum extremum principle which they contended supports inferences derived from Sandström's conjecture, in particular that, if the ocean were driven purely by surface heating, then one wouldn't see the observed small-scale turbulence. However, their arguments do not eliminate the possibility of an ocean circulation that *is* driven by surface heating.

Using energetics, they showed that, in the steady state, energy is input to potential energy from mixing given by the term $\kappa\langle b_z\rangle$, then converted to kinetic energy by the vertical flux of buoyancy $\langle wb\rangle$ and eventually lost to internal energy through mechanical energy dissipation ε where in all cases $\langle\cdot\rangle$ represents total ocean averages. In steady state, the global conversion terms between

different types of energy are

$$\varepsilon = \langle wb \rangle = \kappa \langle b_z \rangle \,. \tag{1}$$

Averaging mixing $\kappa \langle b_z \rangle$ over z they write,

$$\varepsilon \leq \frac{\kappa}{H} \int (b_{top} - b_{bottom}) dxdy \,. \tag{2}$$

Applying fixed temperature boundary conditions, the *maximum extremum* principle implies that the integral on the right-hand side is bounded by a constant Δb, and they conclude that ε scales with the diffusivity κ. This result, that ε vanishes, is their *anti-turbulence theorem*.

However, using calculus of variations, one can show that globally averaged velocity is bounded by the gradient in velocity times a constant prefactor,

$$\left\langle |\mathbf{u}|^2 \right\rangle \leq \frac{2L^2}{\pi^2} \left\langle |\nabla \mathbf{u}|^2 \right\rangle \,, \tag{3}$$

where they considered the ocean periodic in both horizontal directions with period L. Since $\varepsilon = \nu \left\langle |\nabla \mathbf{u}|^2 \right\rangle$ then for circulation,

$$\left\langle |\mathbf{u}|^2 \right\rangle \leq \frac{2L^2}{\pi^2 H} \frac{\kappa}{\nu} \Delta b \,. \tag{4}$$

Keeping the Prandtl number ν/κ fixed, as $\kappa \longrightarrow 0$, then $\left\langle |\mathbf{u}|^2 \right\rangle \leq$ const and Paparella and Young (2002) neither confirms nor denies Sandström's conjecture.

In this paper, we revisit the idea of a buoyancy driven circulation in a simple 1-D thin fluid loop forced by nonuniform heating and two types of boundary conditions: a temperature relaxation boundary condition and a fixed buoyancy flux boundary condition. In §2 we describe the fluid loop formulation and the energetics and form of solutions in the system. In §3 we examine the behavior of steady state fluid flows in the loop subject to heating and cooling at the same geopotential, as well as implications of these solutions for Sandström's conjecture. In §4, we look at type III convection where heating is applied above cooling, and in §5 we look at type I convection where heating is applied below cooling. In this configuration, we find time dependent solutions including periodic orbits, periodic doubling, and chaos-like behavior. Still, we are able to bound quantities with oceanic import, like mechanical energy dissipation and circulation strength. In section §6, we summarize our conclusions, mention a revision of Sandström's conjecture which is true, but does not have the practical applications of Sandström's original conjecture. Finally, we make a few brief comments about what all this means for the global ocean circulation.

2 Fluid Loop formulation

First introduced by Malkus, Howard and Welander (6; 7; 8), the 1-D fluid loop is one of the simplest systems in which to analyze convection. The single dimension of the system is azimuthal, as a result of the thin loop approximation–that the radial thickness of the loop is vanishingly small, and there is no variation in the radial direction. Here, the system is forced by heating and cooling around the loop, with no net heating or cooling. We will also hold the Prandtl number constant.

In our loop, with radius a, v_θ is the azimuthal velocity, Ω is the angular velocity, and angle θ is defined positive in the counterclockwise direction as shown in Figure 3. The loop is oriented

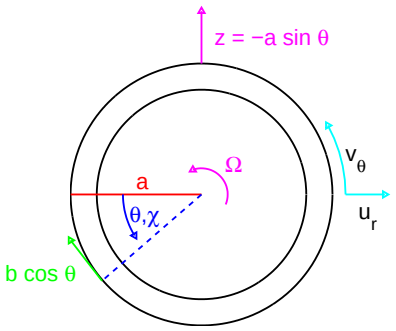

Figure 3: Fluid loop coordinate system and symbol definitions.

vertically so that the z-direction is $a\cos\theta$ and buoyancy acting in the z-direction has component $b\cos\theta$ in the azimuthal direction.

Given this formulation, we may write the velocity of the the fluid as

$$\frac{1}{a}\frac{\partial v_\theta}{\partial \theta} = 0 \,, \qquad v_\theta = a\Omega(t) \,. \tag{5}$$

The buoyancy equation is

$$\frac{\partial b}{\partial t} + \frac{v_\theta}{r}\frac{\partial b}{\partial \theta} = \kappa\left(\frac{\partial^2 b}{\partial r^2} + \frac{1}{r}\frac{\partial b}{\partial r} - \frac{b}{r^2} - \frac{1}{r^2}\frac{\partial^2 b}{\partial \theta^2}\right) \,. \tag{6}$$

We may define our boundary conditions at the inner and outer edges of the thin loop as

$$u_r = 0 \quad \text{at} \quad r_-, r_+ \,, \tag{7}$$

$$\kappa b_r|_{r_-}^{r_+} = \gamma(b^* - b) + F(\theta) \,, \tag{8}$$

where the sources are

$$b^* = g\cos(\theta+\chi) \,, \tag{9}$$

$$F(\theta) = F_0\cos(\theta+\chi) \,. \tag{10}$$

with zero azimuthally averaged forcing, necessary to be able to consider steady states of the system. In all cases below, we will consider $\chi \in [-\pi, \pi]$. Integrating the buoyancy equation (6) in the radial direction and applying boundary condition (8) gives,

$$\frac{\partial b}{\partial t} + \Omega\frac{\partial b}{\partial \theta} = \gamma(b^* - b) + F(\theta) \,. \tag{11}$$

The momentum equation in the radial direction is

$$\frac{\partial u_r}{\partial t} + u_r\frac{\partial u_r}{\partial r} + \frac{v_\theta}{r}\frac{\partial u_r}{\partial \theta} - \frac{v_\theta^2}{r} = -\frac{1}{\rho}\frac{\partial p}{\partial r} + \eta\left(\frac{\partial^2 u_r}{\partial r^2} + \frac{1}{r}\frac{\partial u_r}{\partial r} - \frac{u_r}{r^2} + \frac{1}{r^2}\frac{\partial^2 u_r}{\partial \theta^2} - \frac{2}{r^2}\frac{\partial v_\theta}{\partial \theta}\right) \,, \tag{12}$$

and for a very thin loop, viscosity dominates in the radial direction, then

$$\frac{\partial^2 u_r}{\partial r^2} \approx 0 \,, \tag{13}$$

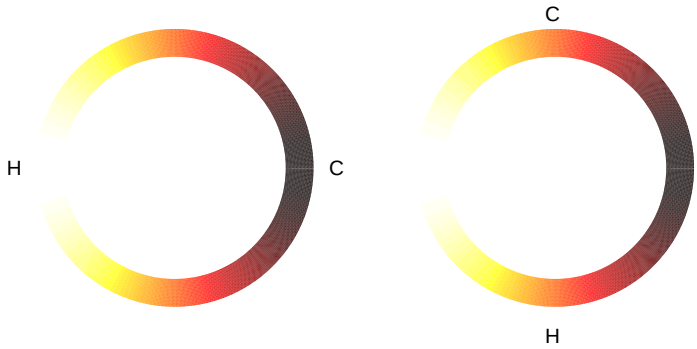

Figure 4: (a) Horizontal convection in the loop ($\chi = 0$). The location of heating maybe thought of as the equator in the ocean, and the location of cooling as the poles. (b) Rayleigh-Bénard convection in the loop ($\chi = 90$). White shading indicates heating; dark shading indicates cooling.

and using the boundary condition (7),

$$u_r = 0 \; . \tag{14}$$

Then the momentum equation in the azimuthal direction becomes

$$\frac{\partial v_\theta}{\partial t} + \frac{v_\theta}{r}\frac{\partial v_\theta}{\partial \theta} = -\frac{1}{r\rho}\frac{\partial p}{\partial \theta} + \eta\left(\frac{\partial^2 v_\theta}{\partial r^2} + \frac{1}{r}\frac{\partial v_\theta}{\partial r} - \frac{v_\theta}{r^2} - \frac{1}{r^2}\frac{\partial^2 v_\theta}{\partial \theta^2}\right) + b\cos\theta \; . \tag{15}$$

From equation (5), we have no variations in velocity or pressure in the azimuthal direction, then integrating in r and θ we have

$$\frac{\partial \Omega}{\partial t} = \frac{1}{2\pi a}\int b\cos\theta d\theta - \eta\Omega \; . \tag{16}$$

Given these sources, when $\chi = 0$ we have heating and cooling applied at the same geopotential level as shown in Figure 2. When $\chi < 0$, heating is applied above cooling as shown in Figure 2. When $\chi > 0$, we have heating applied below cooling in the loop. We will consider these three cases of convection in §3-5.

2.1 Energetics

In this system, kinetic and potential energy are given by

$$KE = \frac{1}{2}a^2\Omega^2 \; , \quad PE = a\cos\theta b \; . \tag{17}$$

By taking $v_\theta \cdot (\text{momentum})$ and integrating around the loop, we can write an evolution equation for kinetic energy as

$$\langle KE \rangle_t = -a\Omega\langle b\cos\theta\rangle - \eta a^2\Omega^2 \; , \tag{18}$$

where $\langle\cdot\rangle = \frac{1}{2\pi}\int \cdot d\theta$. On the right hand side, the first term is the vertical buoyancy flux, the conversion term between kinetic and potential energy, analogous to $\langle wb\rangle$ in the cartesian coordinate system, and the second term is the mechanical energy dissipation ε.

The evolution equation for potential energy is derived by deriving in time $a\langle b\cos\theta\rangle$,

$$\langle PE\rangle_t = a\Omega\langle b\cos\theta\rangle + a\gamma\langle b\sin\theta\rangle + \frac{a}{2}(\gamma g + F_0)\sin\chi \,. \tag{19}$$

The first term in (19) is again the conversion term between kinetic and potential energy. The second term is the source of potential energy through mixing, analogous to $\langle\kappa b_z\rangle$ in the cartesian coordinate system, and the third term representing sources of potential energy through external heating and cooling.

The boundary conditions add no net buoyancy to the system, so the long-time averages of the energy equations (18) and (19) vanish, and we can write

$$\eta a^2\overline{\Omega^2} = a\overline{\Omega\langle b\cos\theta\rangle} = a\gamma\overline{\langle b\sin\theta\rangle} + \frac{a}{2}(\gamma g + F_0)\sin\chi \,. \tag{20}$$

where $\bar{\cdot} = \lim_{T\longrightarrow\infty}\frac{1}{T}\int_0^T \cdot dt$, the long-time average.

Horizontal Convection ($\chi = 0$)

For horizontal convection, equation (20) becomes

$$\eta a^2\overline{\Omega^2} = a\overline{\Omega\langle b\cos\theta\rangle} = a\gamma\overline{\langle b\sin\theta\rangle} \,,$$

which is analogous to Paparella and Young's statement that

$$\varepsilon = \langle wb\rangle = \kappa\langle b_z\rangle \,.$$

However, the same arguments that they used to bound dissipation by a constant times diffusivity do not hold in this case. In particular, the *maximum extremum* principle no longer applies and one cannont bound $\langle b_z\rangle$ nor $a\gamma\overline{\langle b\sin\theta\rangle}$ by a constant, so it is not immediately obvious that the *anti-turbulence theorem* should hold.

Heating above cooling ($\chi < 0$)

In the case of heating above cooling, equation (20) becomes

$$\eta a^2\overline{\Omega^2} = a\overline{\Omega\langle b\cos\theta\rangle} = a\gamma\overline{\langle b\sin\theta\rangle} - \frac{a}{2}(\gamma g + F_0)|\sin\chi| \,.$$

Added buoyancy through either the relaxation temperature or fixed flux boundary condition represents a loss of potential energy to drive the circulation.

Heating below cooling ($\chi > 0$)

For heating below cooling, we have

$$\eta a^2\overline{\Omega^2} = a\overline{\Omega\langle b\cos\theta\rangle} = a\gamma\overline{\langle b\sin\theta\rangle} + \frac{a}{2}(\gamma g + F_0)|\sin\chi| \,.$$

and the buoyancy sources represent a source of potential energy available to drive circulation.

2.2 Solutions for b

Since we are considering solutions in a fluid loop, the buoyancy solution must necessarily be periodic. We can construct the general solution of buoyancy in our equations as an infinite sum of sine and cosine modes,

$$b(t,\theta) = \sum_{n=1}^{\infty} S_n(t)\sin(n\theta) + C_n(t)\cos(n\theta)\ . \tag{21}$$

where S_n and C_n are the amplitudes of the nth mode of buoyancy. Using this form of the solution, equations (16) and (11) become

$$\frac{\partial \Omega}{\partial t} = -\frac{1}{2\pi a}\int C_1(t)\cos^2\theta d\theta - \eta\Omega\ , \tag{22}$$

$$\frac{\partial S_n}{\partial t} = \Omega C_n - \gamma S_n + (\gamma g + F_0)\sin\chi\ , \tag{23}$$

$$\frac{\partial C_n}{\partial t} = -\Omega S_n - \gamma C_n + (\gamma g + F_0)\cos\chi\ . \tag{24}$$

From these equations we can see that only the mode one ($n = 1$) solutions for buoyancy are coupled to equation (22), so the full dynamics of the system are captured using only the mode one solution, irrespective of the form of the forcings, b^* and $F(\theta)$. So dropping the subscript n, we use

$$b(t,\theta) = S(t)\sin\theta + C(t)\cos\theta \tag{25}$$

as our buoyancy solution, and

$$\Omega_t = -\frac{C}{2\pi a}\int \cos^2\theta d\theta - \eta\Omega = -\frac{C}{2a} - \eta\Omega\ , \tag{26}$$

$$S_t = \Omega C - \gamma S + (\gamma g + F_0)\sin\chi\ , \tag{27}$$

$$C_t = -\Omega S - \gamma C + (\gamma g + F_0)\cos\chi\ . \tag{28}$$

are the equations governing our system.

2.3 Nondimensional equations

We rescale the system with the following nondimensionalization,

$$\begin{array}{llll} \hat{\Omega} = \Omega/\gamma, & \hat{S} = \frac{S}{2a\gamma\eta}, & R = \frac{g}{2a\gamma\eta}, & \sigma = \eta/\gamma, \\ \hat{t} = \gamma t, & \hat{C} = \frac{C}{2a\gamma\eta}, & R_F = \frac{F_0}{2a\gamma^2\eta}. & \end{array}$$

where the $\hat{}$ denotes the nondimensional form of a variable. The Rayleigh number is R in our system, and we write an analogous Rayleigh number R_F for the fixed buoyancy flux term.

We rename the variables

$$\begin{array}{ll} X = \hat{\Omega}, & Z = -\hat{C} + r\sin\chi, \\ Y = \hat{S}, & r = R + R_F\ , \end{array}$$

which gives us a new system of equations

$$\dot{X} = \sigma(Y - X) \ , \tag{29}$$

$$\dot{Y} = r\sin\chi X - Y - XZ + r\cos\chi \ , \tag{30}$$

$$\dot{Z} = XY - Z \ . \tag{31}$$

When $\chi = 90$, this is these are the Lorenz equations,[1] where heating and cooling are applied at the bottom and top of the loop respectively. In this system, X is our nondimensional angular velocity, Y is the sine buoyancy mode amplitude, and Z is the cosine buoyancy mode amplitude shifted and flipped. More physical quantities which we will consider are the nondimensional dissipation $\hat{\varepsilon}$, buoyancy flux $\widehat{\langle wb \rangle}$, and mixing $\widehat{\langle \kappa b_z \rangle}$,

$$\hat{\varepsilon} = \sigma X^2 \ , \quad \widehat{\langle wb \rangle} = \sigma XY \ , \quad \widehat{\langle \kappa b_z \rangle} = \sigma Z \ . \tag{33}$$

We will also consider horizontal heat transport, $H_T = \langle v_\theta b \rangle = -a\Omega S/2$. In nondimensional form,

$$\widehat{H_T} = -\sigma(XZ + r\sin\chi X) \ . \tag{34}$$

In the ocean, heating and cooling are applied at the ocean surface which is equivalent to being applied at the same geopotential in the loop, at $\chi = 0$. We will examine the steady state solutions for buoyancy and circulation, their stability, and some of the physical quantities in equation (33) as functions of the Rayleigh numbers defined in our nondimensionalization (§2.3). The goal is to determine the behavior of the solution in the diffusive and nondiffusive limits (small r and large r, respectively).

We will then proceed to consider convection where the heating is applied from above (at $\chi < 0$), the stability of these steady state solutions and their implications for dissipation and circulation. Finally we will consider the case of heating applied below cooling, which is the atmospheric analog since the atmosphere is relatively transparent to the short-wave radiation from the sun, and is heated by long-wave radiation from the Earth. We will again attempt to say something about the behavior of dissipation, circulation and horizontal heat transport as functions of the Rayleigh numbers.

The system of equations (29)-(31) has steady solutions, given by the fixed points (X_0, Y_0, Z_0) satisfying

$$\begin{aligned} Y_0 &= X_0 \ , \\ X_0^3 + (1 - r\sin\chi)X_0 &= r\cos\chi \ , \\ Z_0 &= X_0^2 \ . \end{aligned} \tag{35}$$

If the fixed points are globally stable, then the system has no intrinsic time dependence. If the fixed points are not stable, the solutions of X, Y, and Z to the full equations (29)-(31) can develop time dependence.

[1] The Lorenz system is

$$\begin{aligned} \dot{X} &= \sigma(Y - X) \\ \dot{Y} &= rX - Y - XZ \\ \dot{Z} &= XY - bZ \end{aligned} \tag{32}$$

where b is the aspect ratio of convective cells, typically taken to be 8/3 in the atmosphere, but for a circular fluid loop, $b = 1$ as in our case. Tritton showed that the Lorenz equations could be derived for the loop (9).

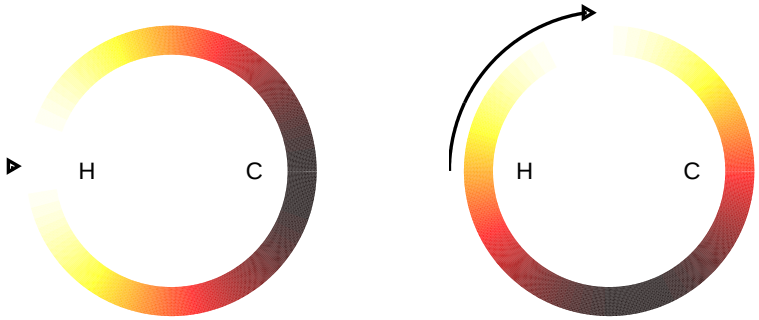

Figure 5: Steady state solutions for horizontal convection $\chi = 0$ with (a) $r = 0.1$ and (b) $r = 100$. "H" and "C" indicate locations of maximal applied heating and cooling and may be thought of as equator and polar regions in the ocean. Colors indicate temperature in the steady state solutions (white hot, dark cold), and arrows indicate the direction and relative magnitudes of circulation for the two cases, small and large r.

3 Horizontal Convection ($\chi = 0$)

For the case of heating and cooling at the same level, also known as horizontal convection, we have $\chi = 0$, for which the fi xed point equation (35) becomes

$$X_0^3 + X_0 = r \ . \tag{36}$$

In the approximation of large and small r, we have the balances

$$X_0^3 \approx r \quad \text{for } r \text{ large} \ , \tag{37}$$

$$X_0 \approx r \quad \text{for } r \text{ small} \ , \tag{38}$$

which give the scalings for the nondimensional, steady state circulation X_0.

Exact solutions are shown in Figure 5. The locations of maximum applied heating and cooling are indicated by the letters "H" and "C", while the colors in the loop show the steady state pattern of temperature in the loop. The arrows show the magnitude and direction of the resultant circulation. In terms of the buoyancy solution in equation (25), the applied forcing for horizontal convection is a cosine mode. For small r (large diffusivity), the resulting steady state pattern of warm and cool water in the loop is dominated by the cosine mode. The pattern is displaced slightly, however, with warm water above the location of heating since the circulation displaces some water, and the diffusion (except in the $r = 0$ limit) does not fully relax the temperature pattern to the applied heating. The circulation is small, but nonzero, resulting from the applied torque of the nonuniform heating, balanced by frictional drag. For large r the pattern of buoyancy is dominated by the sine mode, 90 out-of-phase, and the circulation carries the heat towards the top of the loop and a position of smaller potential energy in the system. The patterns of temperature in the steady state shows the dominance of the forces on the either diffusive, relaxing the temperature pattern to the applied heating, or convective, reducing the torque by moving the light water to the top and the heavy water to the bottom.

3.1 Stability of solutions ($\chi = 0$)

Numerical experiments suggested that the steady solutions were reached for any arbitrary condition. Global stability of a solution means that from any point will move in time towards the steady solution and won't stop till it gets there. This can be shown by constructing a Lyaponov functional of a perturbation (not necessarily small) around the fixed point, then show that the derivative of the Lyaponov functional is negative. Mathematically speaking, we find a function $V(\delta\mathbf{x})$ where $\mathbf{X} = (X,Y,Z)$ and $\mathbf{X} = \mathbf{X_0} + \delta\mathbf{x}$, such that $\dot{V} < 0 \;\forall\; \delta\mathbf{x} \neq \mathbf{0}$, and $\dot{V} = 0$ only for $\delta\mathbf{x} = \mathbf{0}$. We construct a Lyaponov functional for this system, not necessarily unique, as

$$V(\delta x, \delta y, \delta z) = \left(\frac{X_0^2}{\sigma}\right)\delta x^2 + \delta y^2 + \delta z^2 \; . \tag{39}$$

The derivative of V may be rearranged

$$\frac{1}{2}\dot{V} = -\left(\frac{X_0^2}{2}\right)\delta x^2 - \delta y^2 - \frac{1}{2}\delta z^2 - \frac{1}{2}(\delta z - \delta x X_0)^2 \; , \tag{40}$$

from which we can see that

$$\dot{V} \leq 0 \; , \tag{41}$$

so solutions to equation (36) are globally stable.

3.2 Circulation, dissipation and horizontal heat transport ($\chi = 0$)

In the steady state, X_0 is the nondimensional circulation, and nondimensional dissipation and horizontal heat transport are given in the equations in (33). Dissipation and horizontal heat transport scale with r in the large and small limits as

$$\hat{\varepsilon} \approx \sigma r^2 \; , \quad \widehat{H_T} \approx -\sigma r^3 \quad \text{for } r \text{ small} \; , \tag{42}$$

$$\hat{\varepsilon} \approx \sigma r^{2/3} \; , \quad \widehat{H_T} \approx -\sigma r \quad \text{for } r \text{ large} \; . \tag{43}$$

Using the exact solutions of the fixed point equation, the circulation, dissipation and horizontal heat transport shown in Figure 6a-c, and match these scalings in each limit.

In the dimensional form, these quantities are dependent on the choice of boundary conditions used, specified as sources in equation (11), or for the nondimensional fixed point equation as,

$$X_0^3 + X_0 = R \; , \tag{44}$$

$$X_0^3 + X_0 = R_F \; . \tag{45}$$

These two equations are equivalent to setting either $F(\theta) = 0$, or $b^* = 0$ in the dimensional equations (23), which we called restoring-like or fixed flux-like boundary conditions, respectively. The behavior of the dimensional quantities circulation, dissipation and horizontal heat transport

$$\Omega^2 = \gamma^2 X_0^2 \; , \quad \varepsilon = \eta a^2 \Omega^2 \; , \quad H_T = -\sigma a^2 \Omega^3 \; . \tag{46}$$

will be considered as a function of the relaxation timescale, or equivalently diffusivity, γ.

Restoring-like boundary conditions

For restoring-like boundary conditions, we use equation (44) to determine dimensional scalings. In the steady state, dimensional circulation given by $\Omega = \gamma X_0$ scales as

$$\Omega \approx \frac{g}{2a\sigma} \longrightarrow 0 \text{ as } \gamma \longrightarrow \infty \,, \tag{47}$$

$$\Omega \approx \left(\frac{g}{2a\sigma}\right)^{1/3} \gamma^{1/3} \longrightarrow 0 \text{ as } \gamma \longrightarrow 0 \,. \tag{48}$$

So in both the nondiffusive and diffusive limits, circulation vanishes. For dissipation,

$$\varepsilon \approx \frac{g^2}{4\sigma}\gamma^{-1} \longrightarrow 0 \text{ as } \gamma \longrightarrow \infty \,, \tag{49}$$

$$\varepsilon \approx \left(\frac{g^2 a^4 \sigma}{4}\right)^{1/3} \gamma^{5/3} \longrightarrow 0 \text{ as } \gamma \longrightarrow 0 \,. \tag{50}$$

Again, in both limits, dissipation vanishes. Lastly, horizontal heat transport in the steady state,

$$H_T \approx -\frac{g^3}{8a\sigma^2}\gamma^{-3} \longrightarrow 0 \text{ as } \gamma \longrightarrow \infty \,, \tag{51}$$

$$H_T \approx -\left(\frac{ga}{2}\right)\gamma \longrightarrow 0 \text{ as } \gamma \longrightarrow 0 \,, \tag{52}$$

vanishes in both limits. These scalings are shown in Figure 6d-f as indicated by the blue lines.

Fixed flux-like boundary conditions

In the steady state, dimensional circulation given by $\Omega = \gamma X_0$ scales as

$$\Omega \approx \frac{F_0}{2a\sigma}\gamma^{-2} \longrightarrow 0 \text{ as } \gamma \longrightarrow \infty \,, \tag{53}$$

$$\Omega \approx \left(\frac{F_0}{2a\sigma}\right)^{1/3} \longrightarrow \text{ const as } \gamma \longrightarrow 0 \,. \tag{54}$$

So in the diffusive limit, circulation vanishes, but in the nondiffusive limit (as $\gamma \longrightarrow 0$), circulation remains constant. For dissipation,

$$\varepsilon \approx \frac{F_0^2}{4\sigma}\gamma^{-3} \longrightarrow 0 \text{ as } \gamma \longrightarrow \infty \,, \tag{55}$$

$$\varepsilon \approx \left(F_0^2 a^4 \sigma\right)^{1/3} \gamma \longrightarrow 0 \text{ as } \gamma \longrightarrow 0 \,. \tag{56}$$

In both limits, dissipation vanishes. Horizontal heat transport in the steady state,

$$H_T \approx -\frac{F_0^3}{8a\sigma^2}\gamma^{-6} \longrightarrow 0 \text{ as } \gamma \longrightarrow \infty \,, \tag{57}$$

$$H_T \approx -\left(\frac{F_0 a}{2}\right) \longrightarrow \text{ const as } \gamma \longrightarrow 0 \,, \tag{58}$$

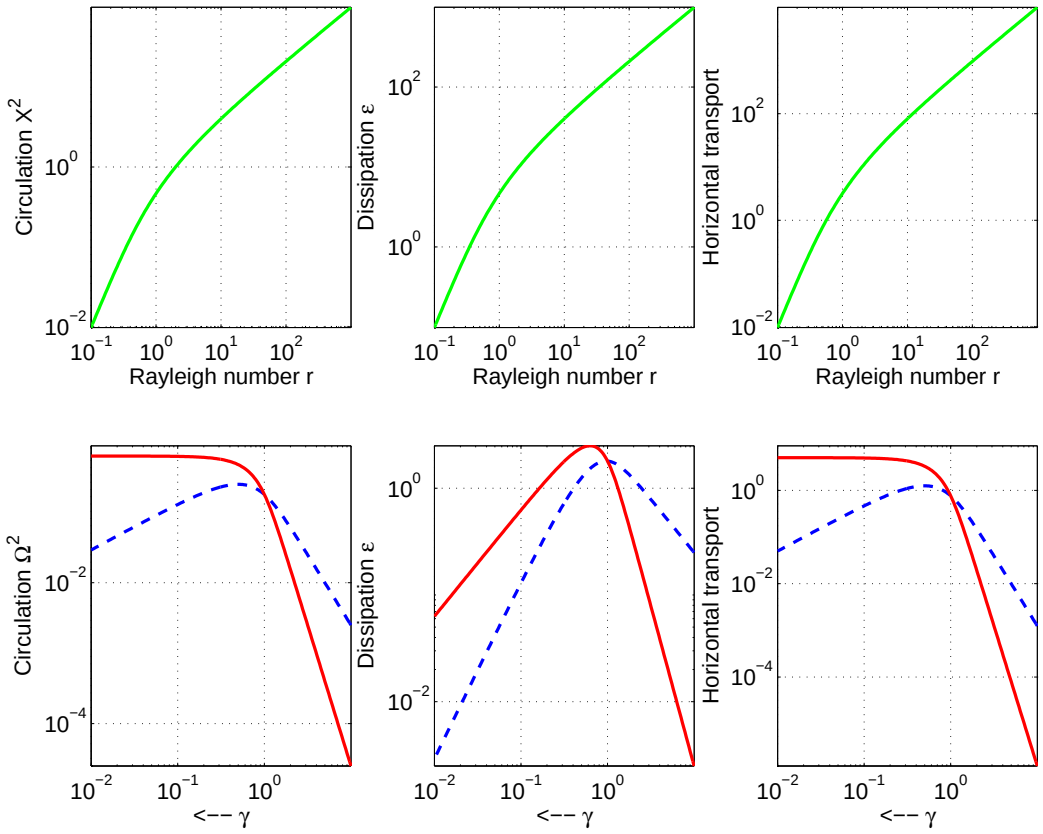

Figure 6: (a)-(c) Nondimensional scaling of circulation, dissipation and horizontal heat transport as functions of the Rayleigh number. (d)-(f) Dimensional scaling of the same, as functions of the relaxation timescale γ. Red solid lines indicate solutions using only fixed buoyancy flux boundary conditions. Blue dashed lines indicate solutions using only the relaxation temperature boundary conditions.

vanishes in the diffusive limit, but is a constant in the nondiffusive limit. These scalings are shown in Figure 6d-f as indicated by the red lines.

In summary, In both cases, dissipation vanishes, in agreement with Paparella and Young's *anti-turbulence theorem*, and for the restoring-like boundary conditions, circulation, and horizontal heat transport vanish in the nondiffusive limit (the oceanic case). However for fixed flux-like boundary conditions, circulation and horizontal heat transport do not vanish.

3.3 Implications for Sandström's conjecture ($\chi = 0$)

1. In the diffusive limit $\gamma \longrightarrow \infty$, the temperature in the steady solution is relaxed to match the applied forcing while, in the nondiffusive limit $\gamma \longrightarrow 0$, the solution has warm water at the top of the loop and cold water at the bottom, towards the limit of minimum potential energy.

2. In the relaxation temperature case ($F(\theta) = 0$, $b^* \neq 0$), dissipation, circulation and horizontal heat transport all vanish in the nondiffusive limit ($\gamma \longrightarrow 0$). This is in accordance with

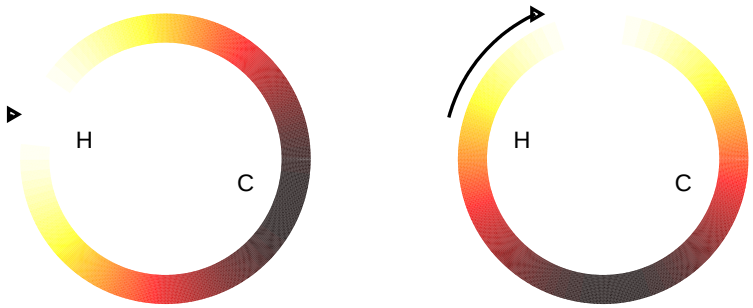

Figure 7: Steady state solutions for heating above cooling $\chi = -15$ with (a) $r = 0.1$ and (b) $r = 100$. "H" and "C" indicate locations of maximal applied heating and cooling. Colors indicate temperature in the steady state solutions, and arrows indicate the direction and relative magnitudes of circulation for the two cases, small and large r.

Sandström's conjecture, that horizontally applied heating cannot drive a circulation.

3. In the fixed buoyancy flux case ($b^* = 0$, $F(\theta) \neq 0$), dissipation still goes to zero in the non-diffusive limit, but circulation and horizontal heat transport saturate at a constant. When diffusion does not carry the applied heating to the location of applied cooling, a circulation must exist to maintain the applied flux. Sandstr öm's conjecture no longer applies given fixed flux boundary conditions. Though heating is still applied horizontally, there is a substantial circulation in the limit of small diffusion.

4 Heating Above Cooling ($\chi < 0$)

For the case of heating above cooling ($\chi < 0$), the fixed point equation (35) is

$$X_0^3 + (1 - r\sin\chi)X_0 = r\cos\chi \,,$$

with $r\sin\chi < 0$. In the approximation of large and small r, we have the balances

$$X_0^3 \approx 1/\tan\chi \quad \text{for } r \text{ large} \,, \tag{59}$$

$$X_0 \approx r\cos\chi \quad \text{for } r \text{ small} \,, \tag{60}$$

which give the scalings for the nondimensional, steady state circulation X_0. In particular, in the large Rayleigh number limit, X_0 scales as a constant, dependent on the angle of applied heating.

The solutions to this cubic polynomial are in Figure 7. Again at low Rayleigh number the circulation is very small and the pattern of heating is very similar to the applied pattern of heating. The circulation results from the balance between applied torque and drag. For large r, the circulation is faster, but not as fast as for horizontal convection at the same Rayleigh number.

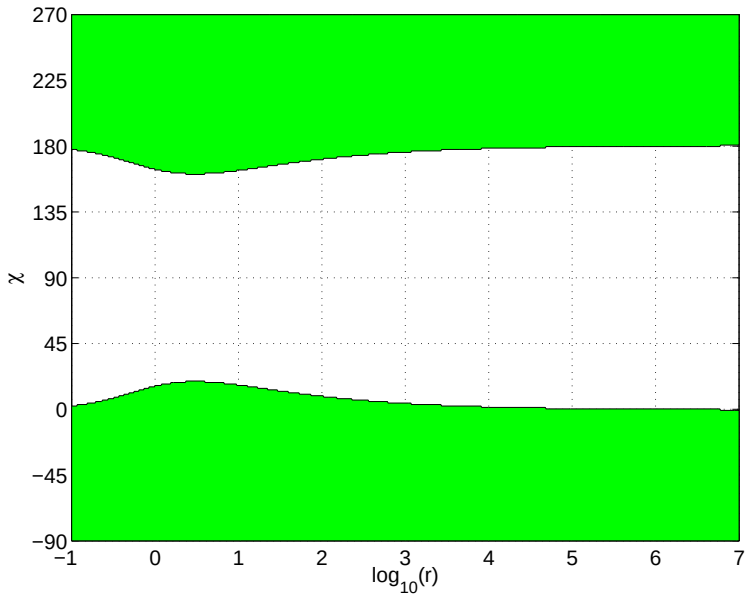

Figure 8: A diagram of the global stability of fi xed points X_0 in $\chi - r$ space given by the condition that $r\sin\chi \leq X_0^2/2$ where X_0 depends in χ and r. The area in green is globally stable.

4.1 Stability of Solutions ($\chi < 0$)

The stability of solutions for heating above cooling is also globally stable, and can be shown using the same Lyaponov functional as for horizontal convection.

$$V(\delta x, \delta y, \delta z) = \left(\frac{X_0^2 - r\sin\chi}{\sigma}\right)\delta x^2 + \delta y^2 + \delta z^2 \ . \tag{61}$$

The derivative of V may be rearranged

$$\frac{1}{2}\dot{V} = -(\frac{X_0^2}{2} - r\sin\chi)\delta x^2 - \delta y^2 - \frac{1}{2}\delta z^2 - \frac{1}{2}(\delta z - \delta x X_0)^2 \ , \tag{62}$$

from which we can see that

$$\dot{V} \leq 0 \tag{63}$$

as long as

$$r\sin\chi \leq \frac{1}{2}X_0^2 \ . \tag{64}$$

For all $\chi < 0$, $r\sin\chi \leq 0 \leq X_0^2/2$ and the condition is met, so the solutions are globally stable. The regions in $\chi - r$ space which are globally stable are shown in Figure 8.

4.2 Circulation, dissipation and horizontal heat transport ($\chi < 0$)

For $\chi < 0$, dissipation and horizontal heat transport scale with r in the large and small limits as

$$\hat{\varepsilon} \approx \sigma r^2\cos^2\chi \ , \quad \widehat{H_T} \approx -\sigma r^3\cos^3\chi \quad \text{for } r \text{ small} \ , \tag{65}$$

$$\hat{\varepsilon} \approx \sigma\cot^2\chi \ , \quad \widehat{H_T} \approx -\sigma\cot^3\chi \quad \text{for } r \text{ large} \ . \tag{66}$$

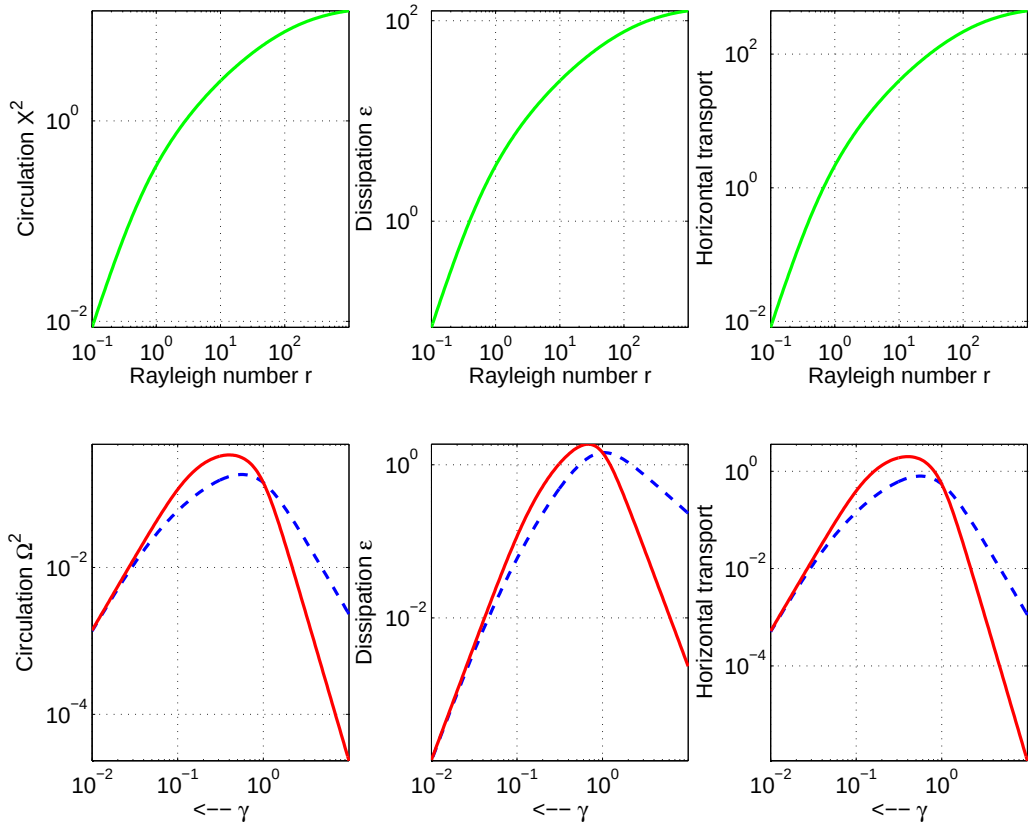

Figure 9: (a)-(c) Nondimensional scaling of circulation, dissipation and horizontal heat transport as functions of the Rayleigh number for heating above cooling ($\chi = -15°$). (d)-(f) Dimensional scaling of the same, as functions of the relaxation timescale γ. Red indicates solutions using only fixed buoyancy flux boundary conditions. Blue indicates solutions using only the relaxation temperature boundary conditions.

These scalings are shown in Figure 9a-c. All three nondimensional quantities saturate at a constant (in r, not in χ) for large r.

In the dimensional form with the quanitites given by the equations in 46, circulation, dissipation and horizontal convection scale as shown in Figure 9d-f. For heating above cooling, with either type of boundary conditions, all dimensional quantities vanish in the diffusive and nondiffusive limits. There exists a circulation for small γ, but it is very weak.

5 Heating Below Cooling ($\chi > 0$)

In this section we will consider heating below cooling, starting first with the special case of heating directly at the bottom of the loop. This case is symmetric across the z-axis and as a result has different characteristics than the other cases for $\chi > 0$. The fixed point equation is, as for $\chi < 0$,

$$X_0^3 + (1 - r\sin\chi)X_0 = r\cos\chi\,, \tag{67}$$

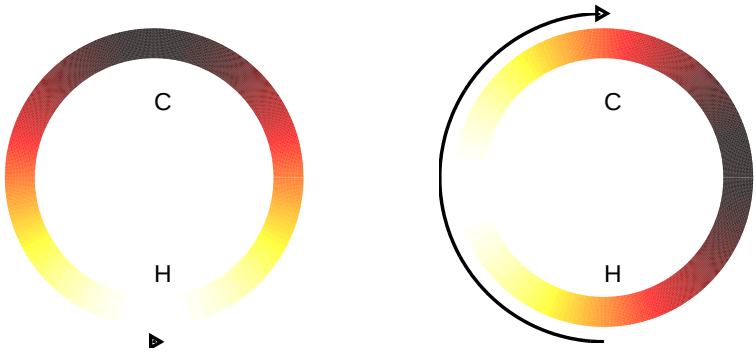

Figure 10: Fixed point solutions for convection with $\chi = 90$ with (a) $r = 0.1$ and (b) $r = 100$. "H" and "C" indicate locations of heating and cooling along the loop. The colors indicate the temperature pattern for a fixed point in the system. Arrows indicate direction and relative magnitude of circulation.

but we will find that for certain parameter ranges of χ and r, the fixed point solutions are not stable, so the solution to the full equations is time dependent.

5.1 Rayleigh-Bénard convection ($\chi = 90$)

We will first consider the special case of heating at the bottom of the loop ($\chi = 90$), called Rayleigh-Bénard convection for which equations (29)-(31) are the Lorenz equations. For this case, the fixed point equation is

$$X_0^3 + (1-r)X_0 = 0\ , \tag{68}$$

with solutions $X_0 = 0$ for all r, and $X_0 = \pm\sqrt{r-1}$ for $r > 1$. This first solution has warm water at the bottom with the heat being carried to the top by diffusion alone. Because the heat is applied symmetrically about the z-axis, there is no applied torque. As diffusion is decreased (r is increased), the $X_0 = 0$ solution becomes unstable (at $r = 1$) and two stable solutions with circulation either clockwise or counterclockwise appear. This is called a pitchfork bifurcation. Two fixed point solutions for small and large r are shown in Figure 10.

For $r = \sigma\frac{\sigma+4}{\sigma-2}$, these two stable solutions become unstable and both simultaneously undergo a subcritical Hopf bifurcation, where the stable solution becomes an unstable limit cycle. The locations of the stable and unstable fixed points, and a diagram of the bifurcation is shown in Figure 11. The pitchfork bifurcation appears as it is called, and the Hopf bifurcations are the two simultaneous from stable to unstable fixed point. More details on this system the Hopf bifurcations in the Lorenz system can be found in Drazin (10).

5.2 General Heating Below Cooling ($\chi \geq 0$)

For the general case of heating below cooling ($\chi > 0$), there are two qualitatively different behaviors that may arise in our system, depending on how close χ is to the symmetric case of $\chi = 90$. For all $\chi > 0$, there is no fixed point solution without circulation since the asymmetrically applied heating creates a torque on the system which, even in cases of large but finite diffusivity (small r), creates a nonzero circulation balancing frictional drag. For larger r, this near zero circulation increases

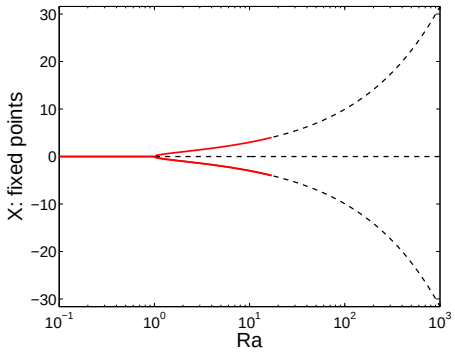

Figure 11: Bifurcation diagram for convection with $\chi = 90$. Solid lines indicate stable fi xed points; dotted lines indicate unstable fi xed points. There is a pitchfork bifurcation at $r = \sim 10$ and two Hopf bifurcations at $r = \sigma(\sigma+4)/(\sigma-2)$.

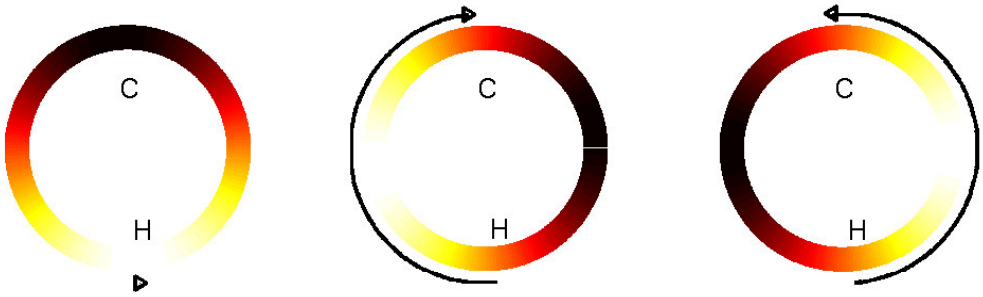

Figure 12: Fixed point solutions for $\chi = 95$. "H" and "C" indicate locations of heating and cooling along the loop. The colors indicate the temperature pattern for a fi xed point in the system. Arrows indicate direction and relative magnitude of circulation.

in magnitude, and two new fi xed points appear out-of-nowhere. The appearance of two new fi xed point solutions from nowhere is called a saddle-node bifurcation. For χ near 90, one of the new fi xed point solutions is stable and the other unstable. For χ further from 90, the two new fi xed points are unstable. This critical angle is approximately $\Delta\chi = 33$, so the region of "χ further from 90" is $|\chi - 90| > 33$.

The three stable zolutions for $\chi = 95$ are shown in Figure 12. At small r, the near-zero circulation is stable and in the direction of applied torque and is the result of the balance between this torque and frictional drag. For larger r, the counterclockwise circulation is in the direction of the torque, so naturally it is larger than the steady state circulation in the opposite direction.

As r increases, the stable clockwise and counterclockwise solutions undergo a Hopf bifurcation, as in the Rayleigh-Bénard case, but not simultaneously. The circulation contrary to the torque goes unstable at smaller r that in the other direction. The bifurcation diagram for $\chi = 95$ is shown in Figure 13.

Numerically computing the fi xed points and their eigenvalues gives us Figure 14, which shows the numbers of stable and unstable fi xed points in $\chi - r$ space. The transitions from 1 to 3 fi xed points are saddle-node bifurcations, and the conversion of a stable fi xed point to an unstable fi xed

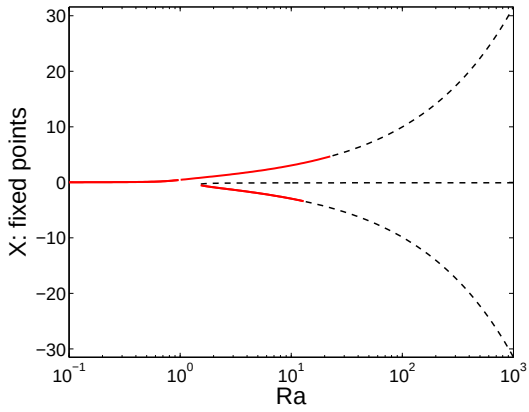

Figure 13: Bifurcation diagram for convection with $\chi = 95$. Solid lines indicate stable fi xed points; dotted lines indicate unstable fi xed points. There is an imperfect bifurcation near $r = 11$ and two Hopf bifurcations near $r = 15$ and $r = 19$.

point is a Hopf bifurcation. The curves for the locations of Hopf and saddle-node bifurcations in $\chi - r$ space may also be computed analytically from the eigenvalues of the fi xed points. The eigenvalues λ of our system are the solutions to the equation, called the characteristic polynomial,

$$det|A - \lambda I| = 0 \,, \tag{69}$$

where A is the linear stability matrix

$$A = \begin{bmatrix} -\sigma & \sigma & 0 \\ r\sin\chi - Z_0 & -1 & -X_0 \\ Y_0 & X_0 & -1 \end{bmatrix} \,, \tag{70}$$

and I is the 3×3 identity matrix. The characteristic polynomial is

$$\lambda^3 + (\sigma+2)\lambda^2 + (2\sigma + 1 + X_0^2 + \sigma(X_0 - r\sin\chi))\lambda + \sigma(1 + 2X_0^2 + X_0 - r\sin\chi) = 0 \,. \tag{71}$$

For a Hopf bifurcation, the real parts of two complex conjugate eigenvalues pass through 0. This is the same as saying that at a Hopf bifurcation, two of the eigenvalues are purely imaginary. Whether the real parts become positive or become negative determines whether or not the Hopf bifurcation is subcritical or supercritical. Then the eigenvalues at a Hopf bifurcation may be called $(\lambda_1, i\omega, -i\omega)$ giving a polynomial which must be equal to the characteristic polynomial for these to be eigenvalues of our system. Then we can solve

$$(\lambda - \lambda_1)(\lambda^2 + \omega^2) = \lambda^3 + (\sigma+2)\lambda^2 + (2\sigma + 1 + X_0^2 + \sigma(X_0 - r\sin\chi))\lambda + \sigma(1 + 2X_0^2 + X_0 - r\sin\chi) \,, \tag{72}$$

or collecting powers of λ,

$$\lambda_1 = -\sigma - 2 \,, \tag{73}$$

$$\omega^2 = 2\sigma + 1 + X_0^2 + \sigma(X_0 - r\sin\chi) \,, \tag{74}$$

$$\lambda_1\omega^2 = -\sigma(1 + 2X_0^2 + X_0 - r\sin\chi) \,. \tag{75}$$

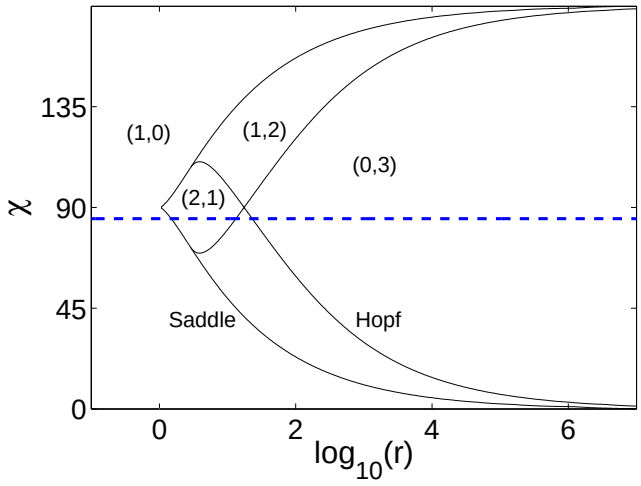

Figure 14: Bifurcation diagram in $\chi - r$ space where (*s*,*u*) indicates the numbers of stable and unstable fixed points in each region, solid lines indicate bifurcations and the dotted line is the slice through *r*-space of $\chi = 95$ for which the bifurcation diagram is shown in Figure 13.

This system of equations may then be solved for $X_0(\chi, r)$ which is the equation of the Hopf bifurcation in $\chi - r$ space. We must also require that $\omega^2 < 0$ since these are two purely imaginary eigenvalues.

Similarly, at a saddle-node bifurcation, one eigenvalue passes through zero giving the polynomial

$$\lambda(\lambda-\lambda_1)(\lambda-\lambda_2) = \lambda^3 + (\sigma+2)\lambda^2 + (2\sigma+1+X_0^2+\sigma(X_0 - r\sin\chi))\lambda + \sigma(1+2X_0^2+X_0 - r\sin\chi) \,, \tag{76}$$

so the last term must be zero, giving

$$-\sigma(1+2X_0^2+X_0 - r\sin\chi) = 0 \,, \tag{77}$$

which may be solves for $X_0(\chi, r)$, the equation of the saddle-node bifurcation. These curves are plotted in Figure 14 and precisely define the transitions between numbers of stable and unstable fixed points.

5.3 Time dependent solutions ($\chi = 45$)

Past both Hopf bifurcations, the system has gone completely unstable, so we use an explicit Runge-Kutta routine in MATLAB to numerically integrate solutions to the system. For the Rayleigh-Bénard case, which is also the Lorenz case, the system quickly becomes chaotic past the Hopf bifurcations, though much further in *r*-space reverts to periodic solutions. For $\chi = 45$, we find that the solutions are initially stable limit cycles and, at higher *r*, develop period doubling and quadrupling, and eventually chaos-like behavior as shown in Figure 15. This is indicative of a supercritical Hopf bifurcation. (In exploring the parameter space near the second Hopf bifurcation for variable χ, it appears as though near $\chi = 90$, the Hopf bifurcation is subcritical and chaos-like behavior develops

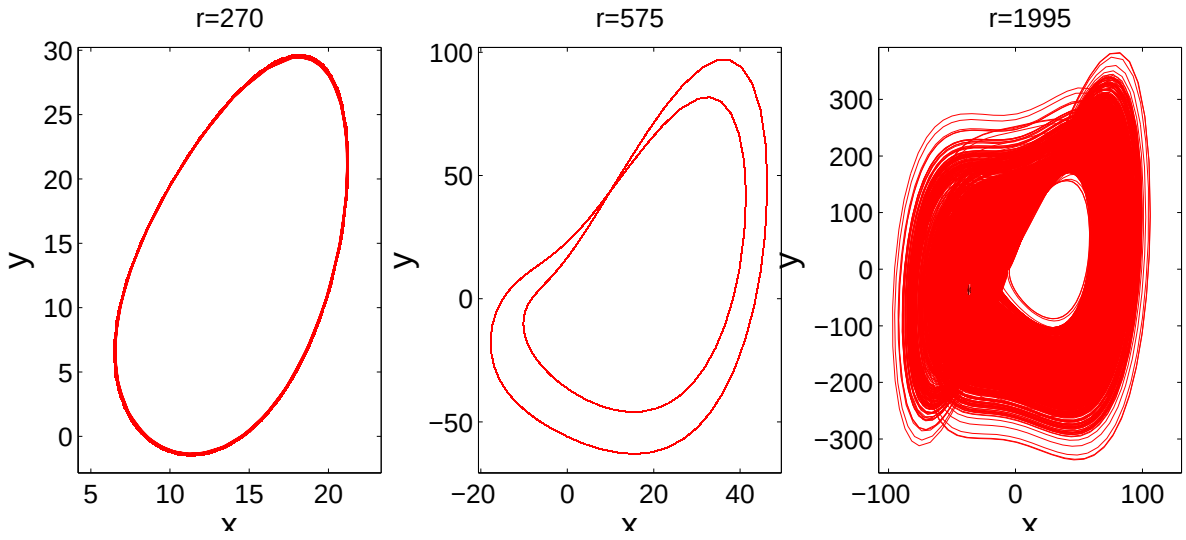

Figure 15: Phase plots of X and Y after a long time, so the initial transient is discounted. (a) For $r = 270$, (b) $r = 575$ and (c) $r = 1995$. These three plots show a stable limit cycle, period doubling and chaotic-like behavior all from the fluid loop for $\chi = 45$.

quickly in r space. Further from $\chi = 90$, by about $\chi = 75$, stable limit cycles are observed and we can conclude that the Hopf bifurcations are supercritical.) Given this sort of behavior, we can no longer explicitly calculate the circulation, dissipation and horizontal heat transport in the system.

5.4 Upper Bound on Circulation and Dissipation ($\chi > 0$)

For the case of heating below cooling ($\chi > 0$), the system exhibits limit cycles, period doubling and chaos-like behavior. However, the long-time averages of circulation, dissipation, and horizontal heat transport can be upper bounded as functions of the Rayleigh number and angle of heating χ. In our nondimensional setup given in §2.3, X is the angular velocity of the fluid. Since we are looking for an upper bound on the magnitude of circulation in the long-time averages of the system, we will look for bounds on X^2. Following the methods of Pétrélis and Pétrélis (11), we find it convenient to define

$$E \equiv \frac{1}{2}(X^2 + Y^2 + Z^2) \tag{78}$$

which has no physical meaning in our system. We also define

$$P \equiv (\sigma + r\sin\chi)XY \ , \tag{79}$$

$$D \equiv \sigma X^2 + \left(Y - \frac{r\cos\chi}{2}\right)^2 + Z^2 - \frac{r^2\cos^2\chi}{4} \ , \tag{80}$$

for which $\dot{E} = P - D$. Then if we can show that $\overline{\dot{E}} = 0$, then $\overline{P} = \overline{D}$ and from the long-time average of equation (29), we know that $\overline{X^2} = \overline{XY}$, a factor in P. So if we can find an upper bound on $\overline{D}$, we will have an upper bound on circulation.

To show that $\overline{\dot{E}} = 0$, we must simply show that E is bounded. For this we follow the methods of Doering and Gibbon (12) and construct a functional L which is decreasing for all (X,Y,Z) outside a finite ellipsoid, which means that all trajectories eventually exist inside this ellipsoid. Defining

$$L \equiv \frac{1}{\sigma}(X + r\cos\chi)^2 + Y^2 + (Z - r\sin\chi - 1)^2 \,, \tag{81}$$

its time derivative is

$$\begin{aligned}\frac{1}{2}\dot{L} &= -X^2 - r\cos\chi X - Y^2 - Z^2 + (r\sin\chi + 1)Z \,, \\ &= -\frac{1}{2}(X + r\cos\chi)^2 - Y^2 - \frac{1}{2}(Z - r\sin\chi - 1)^2 - \frac{1}{2}X^2 - \frac{1}{2}Z^2 + \frac{1}{2}r^2\cos^2\chi + \frac{1}{2}(r\sin\chi + 1)^2 \,.\end{aligned} \tag{82}$$

Then the time derivative of L is bounded by a multiple of L and a constant term,

$$\frac{1}{2}\dot{L} \le -\frac{1}{2}L + \frac{1}{2}(r^2\cos^2\chi + (r\sin\chi + 1)^2) \,, \tag{83}$$

$$\dot{L} \le -L + 2r\sin\chi + 2 \,. \tag{84}$$

Thus outside of the ellipsoid

$$L = 2r\sin\chi + 2 \,, \tag{85}$$

the time derivative of L is negative. Thus all trajectories of X, Y and Z eventually enter this ellipsoid. Then we have shown that E is bounded and we can look for a bound on circulation,

$$\overline{X^2} = \frac{\overline{P}}{\sigma + r\sin\chi} = \frac{\overline{D}}{\sigma + r\sin\chi} \le \frac{D_0}{\sigma + r\sin\chi} \,. \tag{86}$$

The following argument will be to find a small D_0.

Using the background method of Doering and Constantin (13), we can write every solution as the sum of a constant background field and a fluctuating part in time:

$$\mathbf{X}(t) = \mathbf{X_b} + \mathbf{x}(t). \tag{87}$$

Substituting this into equation (80) and taking the long time average, we can write

$$\overline{D} = 2(F(\mathbf{X_b}) - \overline{Q(\mathbf{X_b}, \mathbf{x})}) \,, \tag{88}$$

where

$$F(\mathbf{X_b}) = \frac{1}{2}(\sigma X_b^2 + (Y_b - r\cos\chi/2)^2 + Z_b^2) \,, \tag{89}$$

$$Q(\mathbf{X_b}, \mathbf{x}) = A\hat{x}^2 + \frac{1}{2}\hat{y}^2 + \frac{1}{2}\hat{z}^2 - \frac{1}{2}X_b^2(r\sin\chi - Z_b)^2 - \frac{1}{2}X_b^2Y_b^2 - \frac{L^2}{4A} \,, \tag{90}$$

In equation (90) terms have been gathered as

$$\begin{aligned}A &= \frac{\sigma}{2} - \frac{(Z_b - r\sin\chi - \sigma)^2}{2} - \frac{Y_b^2}{2} \,, \\ L &= X_bY_b^2 + (X_br\sin\chi - X_bZ_b + \frac{1}{2}r\cos\chi)(r\sin\chi + \sigma - Z_b) + \sigma Y_b \,,\end{aligned}$$

and Q has been diagonalized in the fluctuating terms with

$$\begin{aligned}
\hat{x} &= x - \frac{L}{2A} \ , \\
\hat{y} &= y + (Z_b - r\sin\chi - \sigma)x + X_b(Z_b - r\sin\chi) - \frac{1}{2}r\cos\chi \ , \\
\hat{z} &= z - Y_b(X_b + x) \ .
\end{aligned}$$

In order to bound D_0 from above, we must be able to bound Q from below which means that we need $A \geq 0$. For $A \geq 0$, Q is a upward facing paraboloid in (X,Y,Z)-space so the minimum of Q is the apex of the paraboloid. If $A = 0$, then we must have $L = 0$ to avoid singularities in the solution. Since $Q(\mathbf{X_b}, \hat{\mathbf{x}} = 0) \leq Q(\mathbf{X_b}, \hat{\mathbf{x}})$, then

$$\overline{D} \leq D_0 = 2(F(\mathbf{X_b}) - Q(\mathbf{X_b}, \hat{\mathbf{x}} = 0)) \ . \tag{91}$$

Now we would like to pick an $\mathbf{X_b}$ which minimizes D_0. One such solution is

$$\mathbf{X_b} = \left(\frac{r\cos\chi}{2(\sigma - \sqrt{\sigma})}, 0, r\sin\chi + \sigma - \sqrt{\sigma} \right) \tag{92}$$

which gives a relatively tight bound on circulation,

$$\overline{X^2} \leq \frac{D_0}{\sigma + r\sin\chi} = \frac{\frac{1}{4}\frac{\sigma}{(\sigma-\sqrt{\sigma})^2} r^2\cos^2\chi + (r\sin\chi + \sigma - \sqrt{\sigma})^2}{r\sin\chi + \sigma} \ . \tag{93}$$

Using this choice of $\mathbf{X_b}$ gives the bounds for heating below cooling of

$$\overline{X^2} \leq O(r) \ , \tag{94}$$

$$\bar{\tilde{\varepsilon}} \leq O(\sigma r) \ . \tag{95}$$

These bounds, as well as numerically integrated solutions to the equations are shown in Figures 16. The bounds are quite good for large Rayleigh number $r \gg \sigma - \sqrt{\sigma}$. Solutions for $\chi > 0$ have a much more vigorous circulation than for $\chi \leq 0$, but we are still able to bound the circulation and dissipation in the system.

Horizontal heat transport may also be bounded by following the same procedure as above, but letting

$$P' = (\sigma + r\sin\chi)XY + r\cos\chi Y \ , \tag{96}$$

$$D' = \sigma X^2 + Y^2 + Z^2 \ . \tag{97}$$

Finding a bound for $\overline{D'}$ will give a bound for $\overline{P'}$ which may then be compared with the bound for $\overline{P}$ to give a bound for $\overline{Y}$. Then, noting that

$$\overline{\widehat{H_T}} = \overline{\sigma(r\sin\chi X - XZ)} = \overline{\sigma Y} \ , \tag{98}$$

a bound for $\overline{\widehat{H_T}}$ can be found.

The dimensional form of the bounds for circulation and dissipation are shown in Figure 17. Lines are the bounds for different angles and type of boundary conditions, while the stars in corresponding colors are the values computed from integrating the equations. For small γ, equivalently

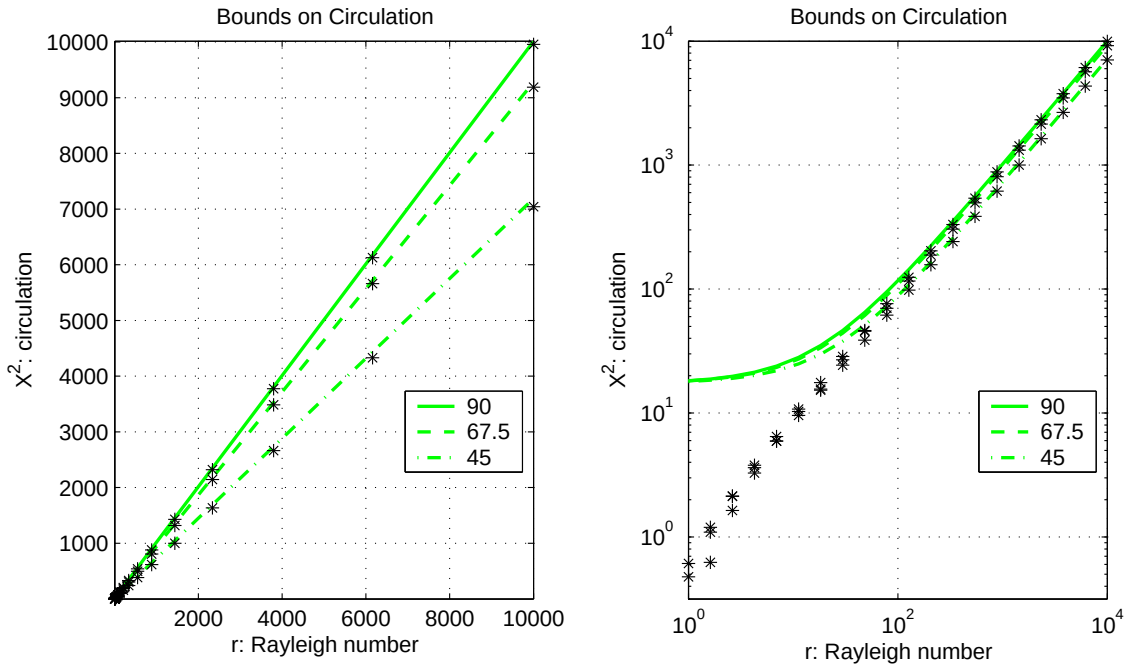

Figure 16: Heating below cooling: Linear and log plots of bounds on circulation for different angles of heating $\chi > 0$. The lines are the bounds given in equation (5.4) for $\chi = 90$, 67.5, and 45, and the stars are estimates of the quantities determined by numerically integrating the equations.

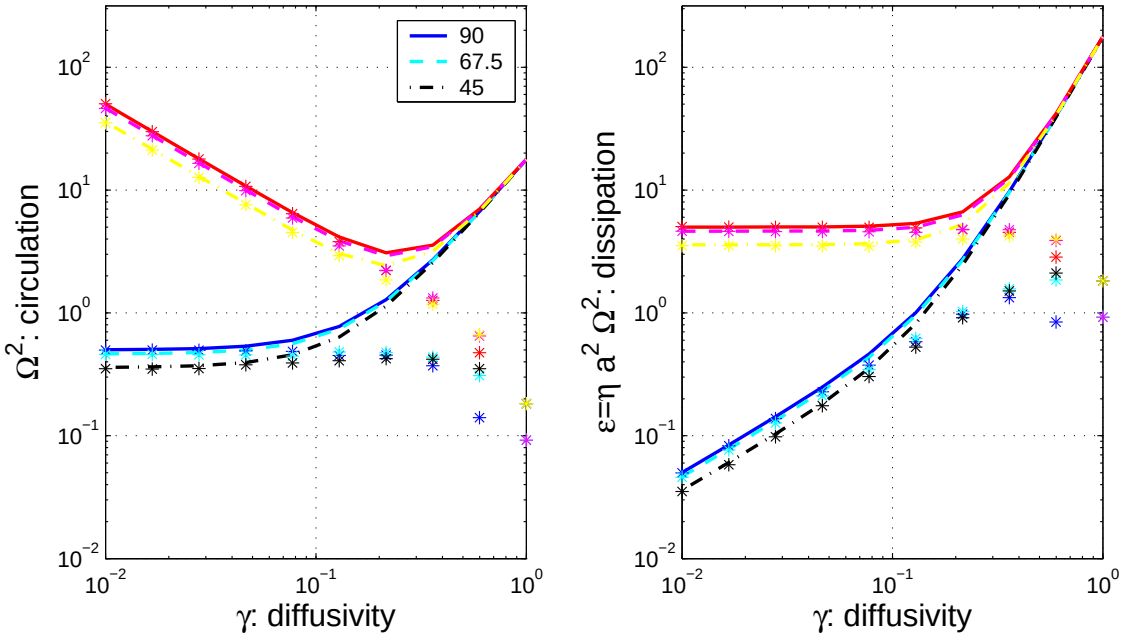

Figure 17: Heating below cooling: Log plots of dimensional bounds on (a) circulation and (b) dissipation, for different boundary conditions (fixed temperature flux in red tones, relaxation temperature in blue tones) and different angles of heating $\chi > 0$. $\chi = 90$ is a solid line, $\chi = 67.5$ is dashed, and $\chi = 45$ is dash-dot. The stars are computed for each χ by numerically integrating the equations.

large Rayleigh number, the bounds are quite good, while for larger γ the bounds are loose. In the nondiffusive limit, the circulation does not disappear and in the case of fixed flux boundary conditions, the circulation increases. The dissipation, in the thermal relaxation case, does disappear, but remains constant in the fixed flux boundary conditions. In either case, the circulation is much more vigorous than the case of horizontal convection.

6 Conclusions

Though the formulation of convection in a 1-D fluid loop is very simple, the possible solutions are diverse and complex. In the oceanic case of horizontal convection, or heating and cooling at the same level, the validity of Sandström's conjecture depends on the nature of the boundary conditions. In particular, using temperature relaxation conditions as in Paparella and Young, and most ocean GCMs, Sandström's conjecture holds: as $\kappa \longrightarrow 0$, circulation vanishes. On the other hand, using fixed buoyancy conditions, even in the limit as diffusivity vanishes, there is a substantial circulation resulting from the differential heating. If Sandström's conjecture were based on sound thermodynamic principles, one would expect it to hold regardless of the nature of the boundary conditions used.

It may be of interest to note that in fact, a variant of Sandström's theorem does hold under both thermal relaxation and fixed flux boundary conditions. In the fluid loop, the location that a parcel experiences heating (at what χ the change in potential energy following a parcel is largest) is not

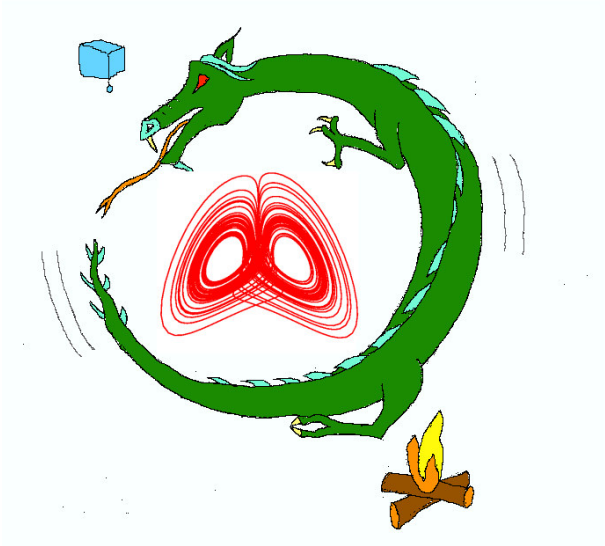

the same as the location of maximally applied heating. If one considers horizontally "experienced" heating (from the point-of-view of a parcel of water), then as $\kappa \longrightarrow 0$, circulation also vanishes. This is not of much practical use in the ocean, however.

In the atmospheric analog of heating below cooling, there exist time dependent solutions with a much more vigorous circulation, though it is still possible to bound the circulation and dissipation in the system as a function of the Rayleigh number. The circulation clearly does not vanish because there is a source of potential energy, the only source which, according to Sandström's conjecture, in the absence of mixing may drive a circulation.

The main point to be taken from all this is that horizontal convection forced with buoyancy conditions (equivalently temperature and salinity) can still drive a finite circulation in the absence of diffusivity, given fixed flux boundary conditions. To motivate the relevance of this statement for the oceans, we note that though sensible heat transfer from the atmosphere to the ocean behaves as a relaxation temperature condition, latent heat and salinity forcing through precipitation and evaporation behave like fixed flux conditions. In fact, latent heating of the ocean is more than twice the magnitude of sensible heating of the ocean, so we would expect fixed buoyancy flux boundary conditions to be more appropriate.

In a fluid loop, a purely thermohaline circulation can exist in the absence of mechanical energy input from wind stress or tidal dissipation. It is not clear that a purely thermohaline circulation cannot exist in the absence of external mechanical energy forcing.

7 Acknowledgments

The author would first like to thank Prof. Raffaele Ferrari of MIT for suggesting the problem and for generous assistance, explanations and suggestions at every step of the way, as well as the Geophysical Fluid Dynamics program at Woods Hole, MA for funding and providing an environment so conducive to study. In addition, many helpful comments and suggestions came from Profs C. Doering, R. Kerswell, N. Lebowitz, and E. Spiegel.

References

[1] W. Young, personal communication (unpublished).

[2] W. H. Munk and C. Wunsch, "Abyssal Recipes II: Energetics of tidal and wind mixing," Deep Sea Res. I **45**, 1977 (1998).

[3] R. X. Huang, "Mixing and energetics of the oceanic thermohaline circulation," J. Phys. Ocean. **29**, 727 (1999).

[4] A. Defant, *Physical Oceanography I* (Pergamon Press, Oxford, 1961), p. 729.

[5] F. Paparella and W. R. Young, "Horizontal convection is non-turbulent," J. Fluid Mech. **466**, 205 (2002).

[6] W. V. R. Malkus, "Non-periodic convection at high and low prandtl number," Mem. Soc. R. Sci. Liège 6^e **IV**, 125 (1972).

[7] P. Welander, "On the oscillatory instability of a differentially heated fluid loop," J. Fluid Mech. **29**, 17 (1967).

[8] P. Welander, in *Large-scale transport processes in oceans and atmosphere*, edited by J. Willebrand and D. L. T. Anderson (NATO ASI Series, Reidel, 1986), pp. 163–200.

[9] D. J. Tritton, *Physical fluid dynamics* (Oxford University Press, Oxford, 1988).

[10] P. G. Drazin, *Nonlinear Systems* (Cambridge University Press, Cambridge, 1992).

[11] F. Pétrélis and N. Pétrélis, "Bounds on the dissipation in the lorenz system," Physics Letters A **326**, 85 (2004).

[12] C. R. Doering and J. D. Gibbon, *Applied Analysis of the Navier-Stokes Equations* (Cambridge University Press, Cambridge, 1995).

[13] C. R. Doering and P. Constantin, "Variational bounds in dissipative systems," Physica D **82**, 221 (1995).